

Robust CIECAM02 Implementation and Numerical Experiment within an International Color Consortium Workflow

Chunghui Kuo, Eric Zeise and Di Lai

2600 Manitou Road, NexPress, Graphic Communication Group, Eastman Kodak, Rochester, New York,
14653–4140

E-mail: chung-hui.kuo@kodak.com

Abstract. *CIECAM02 has gained significant interest within the field of color management for its potential in achieving uniform perceptual color space. However, researchers have identified difficulties in adopting CIECAM02 directly in an International Color Consortium (ICC) workflow as the profile connection space because of the nonlinear post-adaptation response functions as well as the perceptual characteristic functions. In this article, we will address the slight inconsistency in the CIECAM02 derivation under complete illumination adaptation, and a minimized modification on the Hunt–Pointer–Estevez transformation is derived to overcome this difficulty. Furthermore, a robust computation procedure will be suggested to alleviate certain singularities occurring in the original numerical implementation. Finally, we will verify our proposed implementation and compare with the standard procedure within the scheme of the ICC workflow. © 2008 Society for Imaging Science and Technology. [DOI: 10.2352/J.ImagingSci.Technol.(2008)52:2(020603)]*

INTRODUCTION

A color appearance model correctly predicting all of the perceptual color attributes, such as hue, brightness, and chroma, is still being actively pursued by many scientists and engineers to be able to better communicate visual perception with one another.¹ With the current rapid advances in image capture and display technologies, such a model is even more critical to ensure the inter-operability among all equipment. The current international standard supported by the International Color Consortium (ICC) is the latest effort to standardize the color communication specification.² In the ICC specification, a color space, denoted as the Profile Connection Space (PCS), is selected from *CIELAB* or *XYZ*, and each imaging system is described by a color profile in the PCS. The PCS is responsible to connect two different imaging systems: one input device and one output device.

Various color appearance models have been proposed over the years, such as *CIELAB*, the Hunt model, the RLAB model, and the latest CIECAM97s and CIECAM02 models.¹ CIECAM02 is considered to successfully accomplish two objectives: ease of use and offering comprehensive predictions of all attributes of color perception.³ One advantage of adopting CIECAM02 over *CIELAB* is that the predicted hue

angle is better aligned with the perceived hue than that predicted by *CIELAB*, especially in the blue color region.⁴ However, because of the adopted nonlinear post-adaptation function and nonrational definitions of perceived color attributes, researchers have identified several scenarios where the forward and backward algorithms suggested by the CIECAM02 will create numerical irregularities.^{5,6} As a result, special care has to be taken before adopting CIECAM02 directly into the future ICC workflow.^{7,8}

In this article, we will address two issues encountered when adopting CIECAM02 in an ICC workflow: white point under the assumption of complete illumination adaptation, and a numerically robust backward CIECAM02 model. First, although the CIECAM02 suggests a formula to estimate the degree of adaptation, **D**, complete illumination adaptation is usually the preferred choice in the current image reproduction workflow. However, under the current Hunt–Pointer–Estevez transformation defined in CIECAM02, the adapted white point under complete illumination adaptation assumption will not result in the estimated chroma being zero, even though it is very small, i.e., 10^{-5} , but it is unlikely to create problems in actual application when adopting CIECAM02. Nonetheless, we feel that a rigorous color appearance model like CIECAM02 should not produce such a specific prediction with respect to human perception under complete illumination adaptation without experimental verification in the literature. On the other hand, we also believe that the proposed Hunt–Pointer–Estevez transformation resulted from decades of extensive research in human vision. Thus, our first objective is to make as little change as possible on the transformation matrix while imposing the aforementioned constraint of zero chroma. This objective will result in a modified formulation of the Hunt–Pointer–Estevez transformation matrix with minimized impact by solving a simple quadratic optimization with linear constraints.

Second, researchers have indicated that the standard CIECAM02 inverse model has a numerical singularity when converting a point with chroma being zero to *XYZ*.^{5,6} Although this numerical singularity can be avoided by forcing $a=b=0$ at $C=0$, we will show that there still exist numerical difficulties at places with $C \neq 0$ by deriving a set of necessary

Received Feb. 20, 2007; accepted for publication Nov. 26, 2007; published online Apr. 2, 2008.

1062-3701/2008/52(2)/020603/6/\$20.00.

conditions to achieving naturally realizable colors. We propose to solve this numerical difficulty by rearranging the sequence of the CIECAM02 backward model without computing a , b , and obtain R'_a , G'_a , B'_a directly via solving a system of linear equations. We will show that, although mathematically equivalent, this algorithm is more robust numerically by adopting the truncated singular value decomposition algorithm, *TSVD*, in solving the 3×3 linear system as shown in Eqs. (11) and (12) including the colors with zero chroma by predefining a minimum singular value threshold.⁹ Moreover, this matrix formulation will provide a foundation to derive the necessary conditions in CIECAM02 for naturally realizable color. To verify if it is possible to extend the current PCS in an ICC workflow to include CIECAM02, we verify our proposed algorithm in two different routes: $CIELAB(XYZ) \rightarrow CIECAM02 \rightarrow CIELAB(XYZ)$ and $CIECAM02 \rightarrow XYZ(CIELAB) \rightarrow CIECAM02$. In both cases, the initial color spaces are sampled uniformly and form two three-dimensional (3D) cubic grids. The first case starts from the set of non-imaginary colors and identifies the necessary and sufficient conditions for the validity of the CIECAM02 numerical model, but the second case will test the robustness of an inverse model with respect to imaginary colors. We will compare two output gamuts via the standard algorithm and our proposed algorithm.

PROPOSED IMPLEMENTATION

The chromatic adaptation algorithm adopted in the CIECAM02 is a generalized form of the von Kries transformation. The tristimulus values are first mapped to RGB responses using the matrix transformation, M_{CAT02} . Denote the cone responses as R , G , B , and the degree of adaptation as D . It can be easily shown that the RGB responses after chromatic adaptation, R_{cw} , G_{cw} , B_{cw} , of the adapted white point under complete illumination adaptation assumption, i.e., $D=1$, is (100,100,100). The adapted tristimulus values are then mapped to the optimized cone responses via the Hunt–Pointer–Estevez matrix transformation:

$$M_{HPE} = \begin{pmatrix} 0.38971 & 0.68898 & -0.07868 \\ -0.22981 & 1.18340 & 0.04641 \\ 0 & 0 & 1 \end{pmatrix}. \quad (1)$$

The resulting adapted cone responses of the adapted white point, R'_w , G'_w , B'_w , is (100.00001, 100, 100). This will result in nonzero opponent-type responses, a and b , of which chroma is nonzero. Since M_{HPE} optimizes the transformation from tristimulus values to cone responses, our objective is to minimize the modification of M_{HPE} , denoted as δM_{HPE} , while satisfying the constraint of zero chroma. It is obvious that the last two rows of δM_{HPE} are zeros; thus, we can postulate δM_{HPE} to be the following:

$$\delta M_{HPE} = \begin{pmatrix} k_1 & k_2 & k_3 \\ 0 & 0 & 0 \\ 0 & 0 & 0 \end{pmatrix}. \quad (2)$$

Adopting $\|\delta M_{HPE}\|^2 = (k_1^2 + k_2^2 + k_3^2)$ as the cost function quantifying the amount of modification, the modification of M_{HPE} can be reformulated as a simple quadratic programming problem as follows:

$$\begin{aligned} \min & k_1^2 + k_2^2 + k_3^2 \\ \text{s.t.} & k_1 + k_2 + k_3 = 0.00001 \\ & k_1, k_2, k_3 \geq 0. \end{aligned} \quad (3)$$

The solution is $(10^{-5}/3, 10^{-5}/3, 10^{-5}/3)$. By limiting to one extra decimal digit, we propose to modify the Hunt–Pointer–Estevez matrix transformation to be the following:

$$\bar{M}_{HPE} = \begin{pmatrix} 0.389707 & 0.688977 & -0.078684 \\ -0.22981 & 1.18340 & 0.04641 \\ 0 & 0 & 1 \end{pmatrix}. \quad (4)$$

Note that $\bar{M}_{HPE} \rightarrow M_{HPE}$ if they are rounded to the fifth decimal point, and $(a, b) = (0, 0) = (a_c, b_c)$ for the adapted white point under complete illumination adaptation if \bar{M}_{HPE} is adopted in the forward CIECAM02 model.

One numerical singularity that exists in the standard CIECAM02 backward model is that it is necessary to compute the parameter, P_1 , as follows:

$$\begin{aligned} t &= \left(\frac{C}{\sqrt{J/100}(1.64 - 0.29^n)^{0.73}} \right)^{10/9} \geq 0 \\ P_1 &= \frac{(50000/13)N_c N_{cb} e_t}{t}, \end{aligned} \quad (5)$$

where C and J are chroma and lightness, respectively. As a result, if $C=0$, $P_1 \rightarrow \infty$, and it becomes a singular point.⁵ Instead of first solving a and b as suggested by the standard CIECAM02 inverse model, we propose to solve R'_a , G'_a , B'_a directly as explained below. Assuming J , C , and h are known, we can first compute the brightness, A , where $A = A_w(J/100)^{1/cz}$. Note that n , N_c , N_{cb} , c , and z are internal parameters specified in CIECAM02, and they are assumed to be known a priori.^{1,3} Thus, we can construct the first linear equation:

$$2R'_a + G'_a + \frac{1}{20}B'_a = \frac{A}{N_{bb}} + 0.305. \quad (6)$$

Furthermore, because $\sqrt{a^2 + b^2} = a \sec(h) = b \csc(h)$, we can formulate the second linear equation as follows:

$$\begin{aligned} t \left(R'_a + G'_a + \frac{21}{20}B'_a \right) &= ((50000/13)N_c N_{cb} e_t \sec(h))a \\ &= P_2 \left(R'_a - \frac{12}{11}G'_a + \frac{1}{11}B'_a \right) \\ &= ((50000/13)N_c N_{cb} e_t \csc(h))b \end{aligned} \quad (7)$$

$$= \bar{P}_2(R'_a + G'_a - 2B'_a). \quad (8)$$

At last, based on $\tan(h) = b/a$, the final equation can be easily constructed:

$$\tan(h) \left(R'_a - \frac{12}{11}G'_a + \frac{1}{11}B'_a \right) = \frac{1}{9}(R'_a + G'_a - 2B'_a) \quad (9)$$

$$\frac{\cot(h)}{9}(R'_a + G'_a - 2B'_a) = \left(R'_a - \frac{12}{11}G'_a + \frac{1}{11}B'_a \right). \quad (10)$$

Only one equation in the last two cases is selected depending on the relationship between $|\sin(h)|$ and $|\cos(h)|$. If $|\sin(h)| \leq |\cos(h)|$, $\tan(h)$, and $\sec(h)$ are chosen. Otherwise, $\cot(h)$ and $\csc(h)$ are selected. As a result, two 3×3 linear systems with R'_a, G'_a, B'_a being three unknowns can be constructed as shown in the linear system (11) and (12), and solved via the TSVD algorithm.⁹

$$\begin{bmatrix} 2 & 1 & 1/20 \\ P_2 - t & -\frac{12P_2}{11} - t & \frac{P_2}{11} - \frac{21}{20}t \\ \frac{1}{9} - \tan(h) & \frac{1}{9} + \frac{12 \tan(h)}{11} & -\frac{2}{9} - \frac{\tan(h)}{11} \end{bmatrix} \begin{bmatrix} R'_a \\ G'_a \\ B'_a \end{bmatrix} = \begin{bmatrix} \frac{A}{N_{bb}} + 0.305 \\ 0 \\ 0 \end{bmatrix}. \quad (11)$$

$$\begin{bmatrix} 2 & 1 & 1/20 \\ \bar{P}_2 - t & \bar{P}_2 - t & 2\bar{P}_2 - \frac{21}{20}t \\ 1 - \frac{\cot(h)}{9} & -\frac{12}{11} - \frac{\cot(h)}{9} & \frac{1}{11} + \frac{2 \cot(h)}{9} \end{bmatrix} \begin{bmatrix} R'_a \\ G'_a \\ B'_a \end{bmatrix} = \begin{bmatrix} \frac{A}{N_{bb}} + 0.305 \\ 0 \\ 0 \end{bmatrix}. \quad (12)$$

In the case of $C = h = 0$, the linear system can be simplified to be the following:

$$\begin{bmatrix} 2 & 1 & 1/20 \\ 1 & -12/11 & 1/11 \\ 1/9 & 1/9 & -2/9 \end{bmatrix} \begin{bmatrix} R'_a \\ G'_a \\ B'_a \end{bmatrix} = \begin{bmatrix} \frac{A}{N_{bb}} + 0.305 \\ 0 \\ 0 \end{bmatrix}. \quad (13)$$

The singular values of the 3×3 matrix in Eq. (13) are 2.3, 1.39, and 0.22, and its condition number is 10.4. This indicates that it is a well-posed least square problem, and can be

solved reliably. As a result, the singularity caused by the standard CIECAM02 inverse model in computing P_1 , as noted in Eq. (5), can be avoided by adopting our proposed approach. The other advantage of solving a least square problem is that, if the singular values of the Eqs. (11) and (12) become too small, the corresponding singular vectors can be treated as the null space and removed from the solution. Knowing the condition number before inverting a matrix has been shown to result in a numerical robust procedure.⁹ We should note that a necessary condition for a naturally realizable color is $A \geq 0$ as explained in the following section. We can easily extend our proposed CIECAM02 inversion algorithm to consistently resulting in a set of realistic color by imposing the inequality $\min\{R'_a, G'_a, B'_a\} > 0.1$. In this case, Eqs. (11) and (12) can be reformulated again as two least square minimization problems with three inequalities.

NUMERICAL EXPERIMENT

We propose two possibilities for including CIECAM02 into an ICC workflow:

Case 1 PCS remains CIELAB space(or XYZ).

Case 2 CIECAM02 becomes one of the choices for PCS.

Similar to CIELAB space where certain (L^*, a^*, b^*) combinations are not realizable because of the corresponding negative XYZ values, CIECAM02 also contains regions of imaginary colors. Nonetheless, this scenario, by no means, suggests that CIECAM02 is invalid. It is only created by the engineering convenience of a regular multidimensional sampling grid. These imaginary colors in CIELAB are simply projected to the convex set of non-negative XYZ values. In the first case, CIECAM02 is only used to perform gamut mapping, but the final realization is represented in the CIELAB space (or XYZ). Thus, it is necessary to verify the color space transformation from CIELAB to CIECAM02 and back to CIELAB. In the second case, the CIECAM02 color space is sampled by a three-dimensional grid similar to the current ICC PCS implementation. Thus, it is also imperative to identify the region of physically feasible colors within the sampling grid. Moreover, the current profile accuracy estimation is obtained by comparing the color difference between one set of samples initialized in the PCS space and its corresponding points in the same PCS after one round of color mapping. As a result, we will verify another color transformation from CIECAM02 to XYZ(CIELAB) and back to CIECAM02. \bar{M}_{HPE} is adopted in both experiments. Moreover, the symmetric extension of the post-adaptation nonlinearity as suggested by Moroney et al. is adopted in this experiment.³

$$f(x) = 0.1 + \text{sign}(x) \frac{400(F_L|x|/100)^{0.42}}{27.13 + (F_L|x|/100)^{0.42}}, \quad (14)$$

where $x \in \{R', G', B'\}$. Therefore, we can derive the range:

$$-400 < (f(x) - 0.1) < 400. \quad (15)$$

Case 1: CIELAB → CIECAM02 → CIELAB

Various papers have been published addressing this approach.^{5,7,8} The CIELAB color space is first projected to the non-negative XYZ quadrant before mapping to CIECAM02. The necessary condition for the CIECAM02 forward model to succeed is that the achromatic response A is greater or equal to zero, where $A = (2R'_a + G'_a + 1/20B'_a - 0.305)N_{bb}$. The sufficient condition for $A \geq 0$ is

$$\min\{R'_a, G'_a, B'_a\} \geq 0.1 \Leftrightarrow \min\{R', G', B'\} \geq 0$$

$$\Leftrightarrow \bar{M}_{\text{HPE}} \begin{pmatrix} X \\ Y \\ Z \end{pmatrix} \geq 0. \quad (16)$$

We can construct the sufficient condition for valid CIECAM02 forward transformation using \bar{M}_{HPE} in the chromaticity diagram as in Refs. 5 and 6, and they can be represented as the following set of linear inequalities:

$$0.468391x + 0.767661y \geq 0.078684$$

$$-0.27662x + 1.13699y \geq -0.04641$$

$$x + y \leq 1$$

$$x \geq 0, \quad y \geq 0. \quad (17)$$

They are equivalent to the analysis offered by Li and Luo except the slight difference at the first inequality because of the modified first row of the Hunt–Pointer–Estevez matrix.⁵ Note that there exists samples for which $A > 0$ but $\min\{R', G', B'\} < 0$. Because of the adopted symmetric extension as Eq. (14), the forward and backward CIECAM02 transformation are valid at these points.

Our numerical experiment indicates both the standard CIECAM02 inverse model and our proposed model work, which means that no singular value truncation is needed in our proposed inverse model under this scenario. Moreover, the maximal roundtrip error in ΔE_{76} is 1.7×10^{-4} , which is slightly smaller than those reported in Ref. 5. Figure 1 shows the chromaticity diagram of the chromaticity locus, chromaticity regions where $A < 0$, $A \geq 0$ but $\min\{R', G', B'\} < 0$, and the border where $R' = G' = B' = 0$. Figure 2 is the same result represented in the CIELAB color space. It is obvious that the entire chromaticity locus can be safely represented in the CIECAM02 color space even without the symmetric extension of the post-adaptation nonlinearity. This conclusion agrees with Li and Luo,⁵ but differs from that of Tastl et al.⁷ The four active constraints in Eq. (17) form a convex set denoted as S_c . Thus, any convex set with vertices inside S_c is contained in S_c . Therefore, we can conclude that any RGB color space with all primaries satisfying the set of linear inequality constraint (17) can be accurately represented in CIECAM02 color space. At last, the proposed reference media gamut as shown in Fig. 1 also lies entirely within S_c .^{2,7}

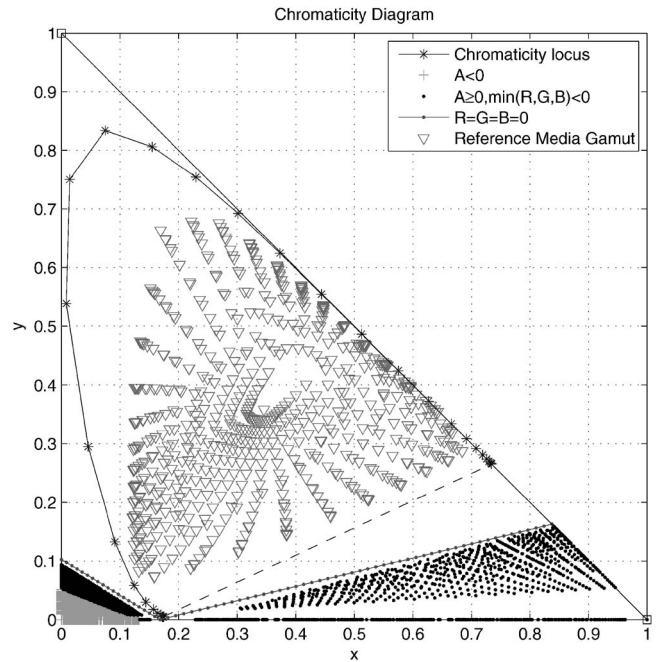


Figure 1. Chromaticity diagram of Case 1 color transformation.

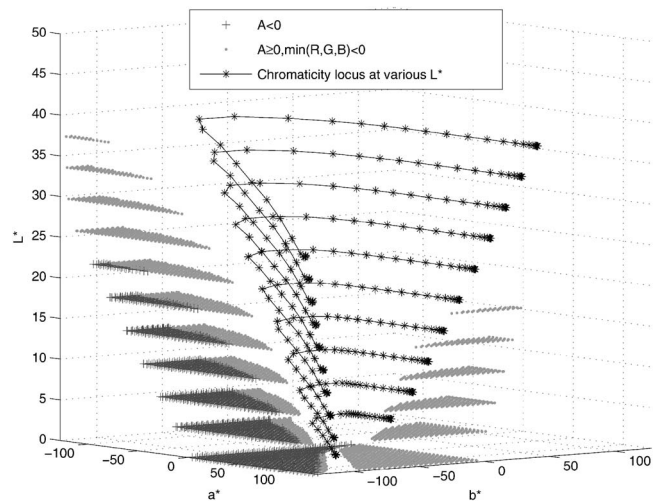


Figure 2. CIELAB 3D graph of Case 1 color transformation.

To verify the effect of singular value truncation, we adopt our TSVD-based inverse model with a lower threshold 0.1 for the computed singular value, and its result is shown in Fig. 3. We can see that the singular value truncation algorithm automatically handles all imaginary colors within the CIECAM02 color space with $A < 0$. Figure 4 shows that same effect in the CIELAB 3D color space.

Case 2: CIECAM02 → XYZ(CIELAB) → CIECAM02

Unlike the first case where the unrealizable CIELAB points are projected to the non-negative XYZ quadrant before applying the CIECAM02 forward transformation as suggested in the ICC specification,² the entire CIECAM02 color cubic is mapped to XYZ color space before the projection can take place. Thus, this process will verify how the standard CIECAM02 inverse model and our proposed model handle

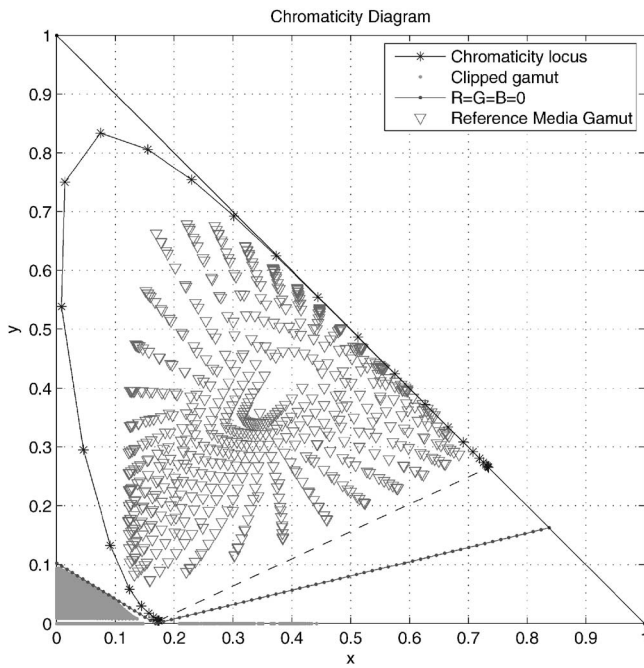


Figure 3. Proposed TSVD inverse model effect in Chromaticity diagram.

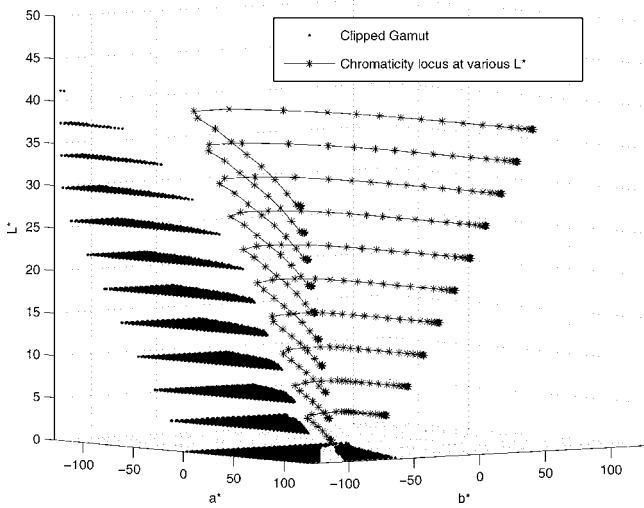


Figure 4. Proposed TSVD inverse model effect in the CIELAB space.

imaginary colors. One constraint which is inactive in the first case is the range of the post-adaptation nonlinear response as listed in Eq. (15). Therefore, a hard clipping function with the upper limit being 399 is imposed on $|R'_a|$, $|G'_a|$, and $|B'_a|$. Furthermore, when the standard CIECAM02 inverse model is used, the derived a and b for any point with chroma $C < 0.01$ will be set automatically to be zero to avoid numerical singularities. When our proposed inverse model is applied, a lower threshold of 0.1 is imposed on the singular values of the derived 3×3 matrix.

It is difficult to derive a set of linear constraints defining the range of valid back-transformation $CIECAM02 \rightarrow XYZ(CIELAB)$ as those shown in Eq. (17) because of the highly nonlinear post-adaptation function and perceptual lightness J , chroma C , and hue h .¹ We will only derive a set

of necessary conditions to produce a non-negative lightness value A , which is necessary for a specific JCh combination representing a naturally realizable color. As noted in Eq. (16), the sufficient condition for $A \geq 0$ is $\min\{R'_a, G'_a, B'_a\} \geq 0.1$. That is to say, the realizable solution of linear systems (11) and (12) is confined in the first quadrant of the (R'_a, G'_a, B'_a) space. Without loss of generality, we will focus our analysis in linear system (11). The constraint on (R'_a, G'_a, B'_a) can be relaxed as

$$\min\{R'_a, G'_a, B'_a\} > 0. \quad (18)$$

As a result, we can deduce that the second and third rows of the system matrix,

$$K_1 = \begin{bmatrix} -12P_2 & P_2 & 21 \\ P_2 - t & -t & -\frac{21}{20}t \end{bmatrix} \quad (19)$$

$$K_2 = \begin{bmatrix} 1 & 1 & 12 \tan(h) & 2 & \tan(h) \\ 9 - \tan(h) & 9 & 11 & -9 & 11 \end{bmatrix}, \quad (20)$$

cannot be all positive or all negative. Let us first consider K_2 . It is obvious that $(1/9 + 12/11 \tan(h))$ and $(-2/9 - \tan(h)/11)$ hold opposite signs if $\tan(h) \geq 0$. When $\tan(h) < 0$, because $(1/9 - \tan(h)) > 0$, the complementary constraint on K_2 can be translated to $(1/9 - 12/11 |\tan(h)|) > 0$ and $(-2/9 + |\tan(h)|/11) > 0$. The two inequalities can be further simplified to two contradicting inequalities: $|\tan(h)| < 11/108$ and $|\tan(h)| > 22/9$. Therefore, the constraint on K_2 is always inactive. As a result, the necessary condition satisfying inequality constraint (18) is that the elements in K_1 hold opposite signs.

Let us analyze the complementary constraint on K_1 , which means that all elements in K_1 are either positive or negative with $t \geq 0$. Let us assume that elements in K_1 are all positive, and three inequalities can be easily derived as follows:

$$0 \leq t < P_2$$

$$0 \leq t < -\frac{12}{11}P_2$$

$$0 \leq t < \frac{20}{231}P_2.$$

Thus, it is impossible for all elements in K_1 to be positive simultaneously. On the other hand, if all elements in K_1 are negative, we can derive the following three inequalities: $t > P_2$, $t > -12/11P_2$, $t > 20/231P_2$. Thus, the necessary condition on JCh to rendering a naturally realizable color is as follows:

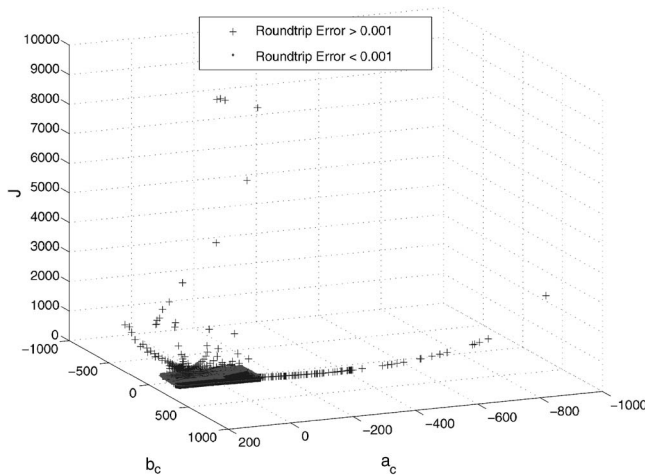


Figure 5. Standard inverse model round trip effect in CIECAM02.

$$t \leq P_2 \quad P_2 \geq 0 \quad (21)$$

$$t \leq \frac{12}{11} |P_2| \quad P_2 < 0. \quad (22)$$

It can be readily seen that, at fixed h , the higher the lightness J , the more saturated chroma C can be achieved.

We first compare the computed $\{R'_a, G'_a, B'_a\}$ from the standard inverse model and the TSVD model. The range of the standard inverse model is from $\{-81.6, -1637.9, -10382.1\}$ to $\{1081.6, 108.5, 3806.7\}$, and that of the TSVD inverse model is from $\{-3.6, -5.0, -53.6\}$ to $\{14.4, 15.7, 77.5\}$, where the corresponding value of the adapted white point is $\{13.05, 13.05, 13.05\}$. It is obvious that the results reported by the standard algorithm are too large. Figures 5 and 6 demonstrate the result of the roundtrip color mapping. The TSVD inverse model automatically controls the output of the inverse function within a reasonable range while the standard inverse model is less robust against imaginary colors within the initial 3D grid points.

CONCLUSION

A constraint is first imposed on the CIECAM02 color appearance model such that the adapted white point should be perceived with zero chroma under complete illumination adaptation. Consequently, a modified Hunt–Pointer–Estevez matrix is derived in Eq. (4). Furthermore, we propose a robust backward numerical implementation based on the TSVD algorithm, which addresses the potential numerical instability of the standard backward model. Two numerical experiments in the previous section indicate that both back-

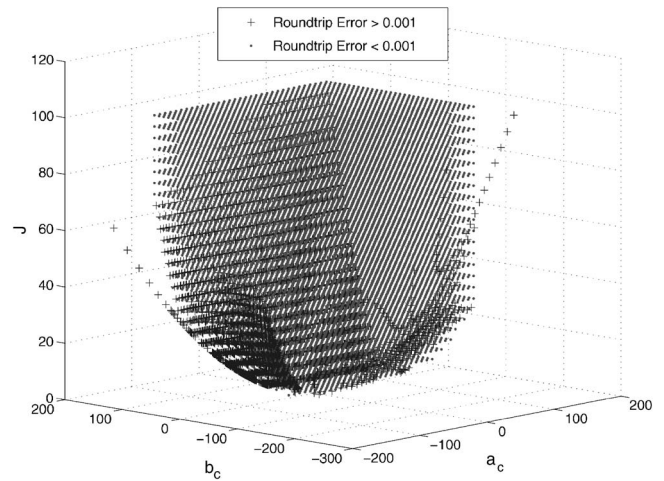


Figure 6. Proposed TSVD inverse model round trip effect in CIECAM02.

ward model implementations achieve high round-trip accuracy under the first $CIELAB \rightarrow CIECAM02 \rightarrow CIELAB$ experiment, where the $CIELAB$ color space is first mapped to the non-negative quadrant of XYZ color space. However, the standard backward model suffers numerical instability in the second numerical experiment, $CIECAM02 \rightarrow CIELAB \rightarrow CIECAM02$, as shown in Fig. 5, where unnaturally high lightness J results from this round-trip experiment. The TSVD-based backward model automatically controls the output within a reasonable range as shown in Fig. 6 where the lower bound of the singular values is set to be 0.1. The numerical singularity at chroma of zero in the standard backward numerical algorithm is also avoided.

REFERENCES

- ¹Mark Fairchild, *Color Appearance Models*, 2nd ed., Wiley-IS&T series in Imaging Science (Wiley, New York, 2005).
- ²International Color Consortium, Specification ICC.1:2004–10, Feb 2005.
- ³N. Moroney, M. D. Fairchild, R. W. G. Hunt, C. Li, M. R. Luo, and T. Newman, “The CIECAM02 Color Appearance Model”, *Proc. IS&T/SID Tenth Color Imaging Conference* (IS&T, Springfield, VA, 2002) pp. 23–27.
- ⁴N. Moroney and Z. Huan, “Field trials of the CIECAM02 color appearance”, *CIE 25th Quadrennium* (CIE Bureau, Vienna, Austria, 2003).
- ⁵C. Li and M. Luo, “Testing the robustness of CIECAM02”, *Color Res. Appl.* **30**, 99–106 (2005).
- ⁶M. Brill, “Irregularity in CIECAM02 and its avoidance”, *Color Res. Appl.* **31**, 142–145 (2006).
- ⁷I. Tastl, M. Bhachech, N. Moroney, and J. Holm, “ICC color management and CIECAM02”, *Proc. IS&T/SID 13th color Imaging Conference* (IS&T, Springfield, VA, 2005) pp. 217–223.
- ⁸R. Guay and M. Shaw, “Dealing with Imaginary Color Encodings in CIECAM02 in an ICC Workflow”, *IS&T/SID 13th Color Imaging Conference* (IS&T, Springfield, VA, 2002), p. 318.
- ⁹P. C. Hansen, “Rank-deficient and discrete ill-posed Problems”, Society for Industrial and Applied Mathematics (SIAM) (1998).